# Deuterium retention behavior of pure and $Y_2O_3$-doped tungsten investigated by nuclear reaction analysis and thermal desorption spectroscopy

M. Zhao[a,b], W. Jacob[b,*], L. Gao[b], A. Manhard[b], T. Dürbeck[b], Z. Zhou[a]

[a] *School of Materials Science and Engineering, University of Science and Technology, Beijing, Beijing 100083, China*

[b] *Max-Planck-Institut für Plasmaphysik, Boltzmannstr. 2, Garching 85748, Germany*

**Abstract:** Pure and $Y_2O_3$-doped tungsten samples were simultaneously exposed to deuterium (D) plasma. The following exposure parameters were investigated: ion energy of 38 eV/D, sample temperatures of 370, 450 and 570 K, and incident fluences of $6\times10^{24}$ and $7.5\times10^{25}$ D/m$^2$. The deuterium retention behavior of these tungsten materials was investigated by nuclear reaction analysis and thermal desorption spectroscopy. After exposure at 450 K $Y_2O_3$-doped tungsten shows a D depth profile comparable with that of pure tungsten. But at each investigated exposure condition $Y_2O_3$-doped tungsten shows a higher total D inventory than pure tungsten. This is attributed to the presence of intrinsic defects with high trapping energies. Investigation of the D retention behavior of four different $Y_2O_3$-doped tungsten materials, which contain the same amount of $Y_2O_3$, but have various microstructures, suggests that sub-micron pores are the underlying intrinsic defects responsible for the appearance of a high temperature D release peak.

**Keywords:** Tungsten, Tungsten Alloys, Deuterium Retention, Plasma-Surface Interaction, Morphology, Thermal Desorption Spectroscopy

**PACS:** 28.52.Fa, 52.40.Hf, 79.20.Rf, 81.05.Ni

| | |
|---|---|
| Published in: | Nuclear Materials and Energy **15** (2018) 32-42. |
| doi: | 10.1016/j.nme.2018.05.016 |
| Submitted: | 27.03.2018 |
| Accepted: | 18.05.2018 |
| Available online: | 03.06.2018 |

## 1. Introduction

Owing to their refractory nature and good thermal properties, tungsten (W) and tungsten alloys are considered as promising candidate materials for plasma-facing components in fusion devices such as ITER and DEMO [1-3]. However, these materials exhibit serious embrittlement at low temperatures particularly in conjunction with recrystallization and neutron irradiation [4-7]. In order to improve the mechanical properties, a variety of advanced tungsten materials are being developed and investigated. One such W material is $Y_2O_3$ dispersion-strengthened tungsten ($W-Y_2O_3$) developed in our previous work [8,9]. This $W-Y_2O_3$ alloy exhibited high fracture strength and obvious ductile behavior at low [8] and high temperatures [9] and good transient thermal shock resistance [9]. As a plasma-facing material (PFM) for fusion reactors, however, its hydrogen retention properties must be known from both fuel balance and radiation safety points of view.

At present, the hydrogen retention properties of $W-Y_2O_3$ are not well known [10]. Specifically, there is a concern of increased retention due to the presence of $Y_2O_3$ particles which could provide additional trapping sites. Published experimental results show either a strong dependence of hydrogen retention on the investigated plasma exposure conditions, such as impact energy, flux, fluence and sample temperature, or on details of the tungsten microstructure, such as grain size, texture, impurities and defect densities [13,14]. For studying the hydrogen retention properties of $W-Y_2O_3$ and clarifying the influence of $Y_2O_3$ particles on its hydrogen retention, we compare its hydrogen retention properties to a pure W material subjected to a similar fabrication process which is assumed to have a similar impurity content and grain structure.

## 2. Experimental details

### 2.1. Materials under investigation

Hydrogen retention was investigated for tungsten materials as listed below:

(1) Pure W: It was provided by Beijing Tian-Long Tungsten & Molybdenum Co., Ltd (TLWM, China)[1]. The nominal purity is above 99.95 %. More than 20 different impurity elements were identified in its chemical composition list [10]. The typical grain size parallel to the specimen surface is 1−5 μm, while perpendicular to the specimen surface the size is 0.4−1.6 μm. The material has no visible open pores [10]. The pure W material used in this work is from the same production batch as the comparable pure W material described in [10].

(2) $W-Y_2O_3$: In this work, three different $W-Y_2O_3$ materials were investigated. We used as-sintered, as-rolled and spark-plasma-sintered (SPS-ed) $W-Y_2O_3$, respectively. All of them were fabricated from mechanically alloyed W (purity: 99.97 wt.%, average grain size: 2 μm) and 1 wt.% Y powders (purity: 99.9 wt.%, average grain size: 48 μm). All Y was transformed into $Y_2O_3$ due to reaction with oxygen during the fabrication process. The content of the formed $Y_2O_3$ in $W-Y_2O_3$ is 1.24 wt.% theoretically. The detailed procedure for mechanical alloying can be found in [15]. Due to the contamination with grinding media and/or the leakage of atmosphere during ball milling process $W-Y_2O_3$ has small traces of extra impurities (in weight ppm), such as Mo around 300 (≈ 0.058 at.%), C around 280 (≈ 0.43 at.% ) and O around 2500 (≈ 2.90 at.%) [8]. In comparison to the intrinsic C and O impurities of the investigated pure W specimen, the amount of C in $W-Y_2O_3$ increased by an

[1] TLWM was fused in 2015 with Refractory Materials & Ceramics Branch of Advanced Technology & Materials Co., Ltd. (AT&M) and is now doing business under the name ATTL Advanced Materials Co., Ltd. (ATTL).

order of magnitude, and more significantly, the amount of O increased by two orders of magnitude. However, the vast majority of the additional O in W−$Y_2O_3$ has reacted with Y to form the high-temperature-stable $Y_2O_3$ particles and most of the C has reacted to WC [8].

As-sintered W−$Y_2O_3$ was produced by cold isostatic pressing followed by high temperature sintering in flowing $H_2$. Afterwards, as-sintered W−$Y_2O_3$ was cut into two pieces. One of them was additionally subjected to a similar hot rolling and stress relief procedure as pure W (in the following called "as-rolled W−$Y_2O_3$"). As-sintered and as-rolled W−$Y_2O_3$ were fabricated in collaboration with TLWM. The detailed production routes for the two W−$Y_2O_3$ materials can be found in [8]. As-sintered W−$Y_2O_3$ consists of polyhedral tungsten grains (average grain size: 4 μm), spherical dispersed $Y_2O_3$ particles (size distribution: ~0.68 and 1.1−1.7 μm) and nano-sized/sub-micron pores (volume fraction: 1.1 %). $Y_2O_3$ particles and residual pores are predominantly distributed along tungsten grain boundaries. After rolling, tungsten grains and $Y_2O_3$ particles were elongated along the rolling direction, the porosity was reduced to 0.7 %. As-rolled W−$Y_2O_3$ exhibits a similar grain structure as pure W. The residual pores in as-rolled W−$Y_2O_3$ have a size of several hundred nanometers and are located at $Y_2O_3$-W interfaces [10].

SPS-ed W−$Y_2O_3$ was fabricated using spark plasma sintering (SPS) technique in vacuum. Detailed fabrication routes can be found in [16]. Dispersed $Y_2O_3$ particles are distributed both inside individual tungsten grains and along tungsten grain boundaries. $Y_2O_3$ particles at tungsten grain boundaries exhibit a multi-modal size distribution with peaks centered at 0.13, 0.24 and 0.46 μm, respectively [16]. The tungsten grains exhibits an isotropic microstructure with an average grain size of 0.77 μm. This material has a porosity of 0.7 %.

### 2.2. Specimen preparation and plasma exposure

Prior to implantation samples were cut by electric discharge machining to dimensions of 10×10×0.8 $mm^3$. The exposed surface is parallel to the plate surface, i.e., parallel to the rolling direction. The residue from the wire cutting process was removed by coarse grinding of the sample with SiC sand paper. As described in [17], the specimens were then polished to mirror finish with a final polishing step involving chemical etching to remove the distorted surface layer due to the previous mechanical polishing steps. After polishing and ultrasonic cleaning the specimens were degassed in a high-vacuum furnace at a pressure of $10^{-4}$ Pa and a temperature of 1200 K for 2 h. This temperature is high enough to remove polishing residue from the surface, as well as some impurities, vacancies and dislocations in the near surface layer without leading to recrystallization or grain growth.

All of the different specimen types were exposed simultaneously to deuterium plasma using the well-quantified plasma device PlaQ [18]. For the used exposure conditions, i.e., 1.0 Pa $D_2$ gas pressure, the impinging ion flux is composed of 94 % $D_3^+$ ions, 3 % $D_2^+$ ions and 3 % $D^+$ ions. Details of PlaQ can be found in [18]. The incident D flux was fixed at ~$9\times10^{19}$ D/($m^2$ s) and the ion energy at 115 eV. This ion energy corresponds to an energy of 38 eV /D for the dominant ion species ($D_3^+$). Most of the samples were irradiated to a fixed fluence of $6\times10^{24}$ D/$m^2$. One additional experiment was performed with an exposure of $7.5\times10^{25}$ D/$m^2$. If not stated otherwise, all data correspond to the lower fluence of $6\times10^{24}$ D/$m^2$. The implantation temperatures investigated here were 370, 450 and 570 K. These exposure temperatures are chosen to allow comparison with prior work, in particular with the data published in Ref. [10]. For 370 and 450 K, an open circuit thermostat with silicon oil was used to stabilize the sample holder temperature. For higher temperatures, e.g., 570 K the sample holder was radiation heated by a BORALECTRIC® heater element. The sample holder temperature was measured independently by a thermocouple that is pressed

against the sample holder from below. Additionally, the temperature of the plasma-facing surface was directly measured by a microbolometer infrared camera.

### 2.3. Nuclear reaction analysis (NRA)

The D amounts and the depth profiles in the near surface region were measured by ion beam analysis using the D ($^3$He, p) $^4$He nuclear reaction at different $^3$He energies. For all NRA measurements reported here 7 different $^3$He energies in the range from 0.5 to 4.5 MeV were used. The cross section of this nuclear reaction peaks at ~620 keV $^3$He energy [19]. The depth, which is probed for D, depends on the primary energy since the $^3$He ions lose energy as they penetrate the target. The applied experimental conditions yield a maximum information depth of about 8 μm. The produced high energy protons from NRA were counted using a thick, large-angle solid state detector at a scattering angle of 135° equipped with a parabolic slit reducing the solid angle to 29.9 msr (±3 %). The protons from the nuclear reaction at different $^3$He energies were evaluated to obtain the underlying depth profile using NRADC which is a sophisticated analysis program applying Bayesian statistics [20]. These NRA measurements were carried out 4~7 days after deuterium implantation. The total accumulated D inventory was calculated from the integration of the depth profile. It represents an average value over the analyzing spot which has an area of 1 mm$^2$. More details on the experimental set-up for the nuclear reaction analysis (NRA), the depth resolution and the data evaluation can be found in [14,20,21]. Due to the limited depth resolution of the applied NRA method the D depth profiles are shown in a histogram-type representation where each layer corresponds to the averaged D content inside the respective layer. Furthermore, depending on the real depth profile and the information content of the measured raw data (proton spectra) the number of independent layers resulting from the NRADC analysis can be lower than the number of used projectile energies (for details see [20]). The error bars shown in the D depth profiles are from the NRADC data evaluation [20] and comprise only the statistical uncertainty from the raw data and the model evaluation. The absolute D amounts are additionally afflicted with the uncertainty of the calibration of the solid angle of the proton detector (3 %, see above) and the uncertainty of the published cross section (5 %, see [19]). The latter two uncertainties are included in the absolute D amounts listed in Table 1.

| Sample | $T_{sample}$ (K) | Fluence ($10^{24}$ D/m$^2$) | NRA ($10^{20}$ D/m$^2$) | TDS ($10^{20}$ D/m$^2$) | HD (%) | Heavy water (%) | $F_{NRA}$ | $F_Y$ |
|---|---|---|---|---|---|---|---|---|
| Pure W | 370 | 6 | 6.5±0.5 | 5.5±0.5 | 5.8 | 8.6 | 1.18±0.14 | − |
| | 450 | 6 | 9.5±0.7 | 10.7±0.6 | 3.5 | 3.7 | 0.89±0.08 | − |
| | 570 | 6 | 0.5±0.05 | 1.8±0.4 | 10.0 | 19.7 | 0.28±0.06 | − |
| | 450 | 75 | 7.1±0.5 | 16.9±0.8 | 3.1 | 2.8 | 0.42±0.04 | − |
| As-rolled W−$Y_2O_3$ | 370 | 6 | 7.0±0.6 | 6.5±0.5 | 15.0 | 6.7 | 1.08±0.12 | 1.2±0.15 |
| | 450 | 6 | 9.4±0.7 | 14.3±0.7 | 12.2 | 3.0 | 0.66±0.06 | 1.3±0.10 |
| | 570 | 6 | 1.3±0.1 | 6.5±0.5 | 31.3 | 6.8 | 0.20±0.02 | 3.6±0.78 |
| | 450 | 75 | 6.6±0.5 | 25.4±1.1 | 13.9 | 1.9 | 0.26±0.02 | 1.5±0.10 |
| SPSed W−$Y_2O_3$ unannealed | 450 | 6 | 13.6±0.9 | 14.4±0.6 | 1.1 | 0.6 | 0.94±0.07 | − |
| SPSed W−$Y_2O_3$ (annealed) | 450 | 6 | 20.6±1.3 | 20.2±0.8 | 1.1. | 0.6 | 1.02±0.07 | − |

**Table 1:** Total amount of retained D determined by NRA and TDS in pure W, as-rolled W−$Y_2O_3$, and SPSed W−$Y_2O_3$ exposed to different fluences at different sample temperatures. The retained D amounts determined by NRA for samples exposed to a fluence of $6\times10^{24}$ D/m$^2$ were previously published in [10]. The estimated contributions from heavy water (HDO and $D_2O$) and HD to total D release is also listed. $F_{NRA}$ is the fraction of the total D amount (measured by TDS) found within the NRA analysis depth. $F_Y$ is the ratio of the total D amount (measured by TDS) in as-rolled W−$Y_2O_3$ and in pure W ($F_Y = D_{W\text{-}Y2O3}/D_{pure\text{-}W}$) for the identical exposure condition. The listed uncertainties of the total amounts include the contributions as explained in sections 2.3 and 2.4. The uncertainties of the $F_{NRA}$ and $F_Y$ ratios are the corresponding calculated propagated uncertainties.

### 2.4. Thermal desorption spectroscopy (TDS)

All TDS measurements were performed 2~3 months after the NRA measurements in the device named "TESS". A basic description of TESS is given in [22]. One point that should be mentioned here is that a possible loss of deuterium during this storage time between NRA and TDS measurement could occur [23]. The specimens were loaded into the quartz tube of TESS which was pumped for approximately 4 hours before it was connected to the main analysis chamber. After another ~10 hours of pumping the base vacuum of the order of $10^{-8}$ Pa was reached. Only if the background signals of relevant mass channels were sufficiently low the measurement procedure was started. Prior to an experiment the region of the glass tube that was later used for the TDS measurements was heated to 1320 K for 1 hour to desorb gases adsorbed to the inner walls of the glass tube. This procedure minimizes the contribution of background gases to the signals recorded during TDS measurements. Some more details on the TDS measurements procedure and data acquisition can be found in [24]. For all shown cases, background measurements with an empty glass tube for species of interest, in particular for water-related signals, applying identical heating ramps as for the measurements are significantly lower than signals with samples. Background TDS spectra without samples are recorded in regular intervals to check the status of the experimental set-up. The specimen in the measurement position was radiation-heated by a tubular oven that was programmed for a linear temperature ramp. The oven was heated from room temperature to 1320 K at a heating rate of 15 K/min. The maximum temperature ($T_{max}$) of 1320 K was maintained for at least one hour to allow for additional release of trapped D. The maximum temperature of 1320 K is determined by technical constraints of the device. The deuterium release rate decreased to zero before $T_{max}$ was reached for all pure W specimens. But for $W-Y_2O_3$ specimens exposed at all conditions a non-negligible deuterium release rate was still observed after reaching $T_{max}$. The D release rate decreased with time for holding the sample at $T_{max}$, but it did not reach zero even after one hour holding at $T_{max}$. This means the total deuterium inventory of $W-Y_2O_3$ measured by TDS is to some small extent underestimated. For a number of samples the remaining D amount was checked by NRA. In all cases investigated the NRA signal was at background level meaning that a possible remaining D content is below the NRA detection limit which is about $10^{-5}$ D/W. Nevertheless, the desorption spectra and total desorbed D amounts can be directly compared between samples because identical heating ramps were used.

The temperature response of the samples to the linear oven temperature ramp was calibrated in independent experiments by a thermocouple spot-welded to samples made of the different types of tungsten materials used. For an oven temperature ramp of 15 K/min, there is a significant delay between the oven temperature and the specimen temperature at the start of the T ramp. This is due to the relatively high heat capacity of the tungsten specimen together with their very low absorption coefficient for infrared radiation in particular at low temperatures. This leads to a nonlinear sample heating rate up to about 600 K. At the beginning of the temperature ramp, the sample heating rate is significantly lower than the oven temperature ramp. For oven temperature higher than about 400 K sample heating becomes more efficient and up to about 600 K the sample ramp is higher than the oven ramp. For temperatures higher than 600 K the oven and sample temperature ramps are the same. As a result, over the whole range the oven temperature is significantly higher than the true sample temperature. At low oven temperature the difference can reach up to 240 K. For temperatures larger than about 600 K the offset reduces to 50−60 K and remains constant at this value up to $T_{max}$. Here, we should note that variations in the linearity of the heating rate lead to changes in desorption peak heights and possibly also to shifts of the peak position. In general, higher heating rates produce stronger desorption peaks and shift the peak maxima to

higher temperature. But with respect to the measurement of total D inventory variations of the temperature ramp rates are no real issue, because the total retained D amounts are determined by integration of the D release rates measured as a function of time. Because furthermore, the sample temperature ramps for different samples are comparable, the peak shapes and position can also be compared with each other. However, for comparison of the TDS spectra shown here with those of other experimental set-ups the nonlinearity of the sample temperature ramp up to about 600 K has to be taken into account.

During heating, HD (mass 3), $D_2$ (mass 4), HDO (mass 19), $D_2O$ (mass 20), and other mass channels were recorded by a quadrupole mass spectrometer (QMS, Pfeiffer DMM422). The QMS signal for $D_2$ was calibrated to absolute desorption fluxes by an independent measurement using a calibrated leak (Laco Technologies). The gas inlet for the leak valve is not at the sample position, but on a flange in the main vacuum chamber which is at a position comparable to the flange at which the quartz tube of TESS is attached to the main vacuum chamber [22]. In the past we have compared the calibration factors for $H_2$, $D_2$, and HD. This calibration procedure is described in detail in [24]. The most recent calibration procedure including HD has resulted in a comparable calibration factor for HD as for $D_2$. Therefore, in the experiments presented here the same calibration factor was used for HD and $D_2$. The calibration factors for all gases vary slightly with time due to ageing of the detector in the QMS. Therefore, the calibration factor for $D_2$ is determined on a regular basis. For heavy water isotopologues, i.e., HDO and $D_2O$, it is extremely difficult to determine reliable calibration factors due to the fact that water molecules have a significant, strongly temperature-dependent sticking coefficient and can get permanently lost to the chamber walls on the way to the QMS. The tabulated sensitivity factor of $H_2$ is 0.44 and for $H_2O$ this value is 0.90 [25,26]. The ratio of the latter two sensitivity factors was assumed in the evaluation of the current data to enable an estimate of the D release in form of water isotopologues. Because we have no relative sensitivity factors for HDO and $D_2O$ we applied the same values as for $H_2O$. It should be emphasized that the estimate of the D release in form of water is afflicted with a relative large uncertainty which is determined by the unknown loss to the chamber walls during transport. As uncertainty for the total D amount determined from the TDS data we assumed a relative uncertainty of 4 % for the D released in form of $D_2$ and HD and an uncertainty of 100% for the contribution from water isotopologues. The propagated uncertainty from these two quantities is listed in Table 1.

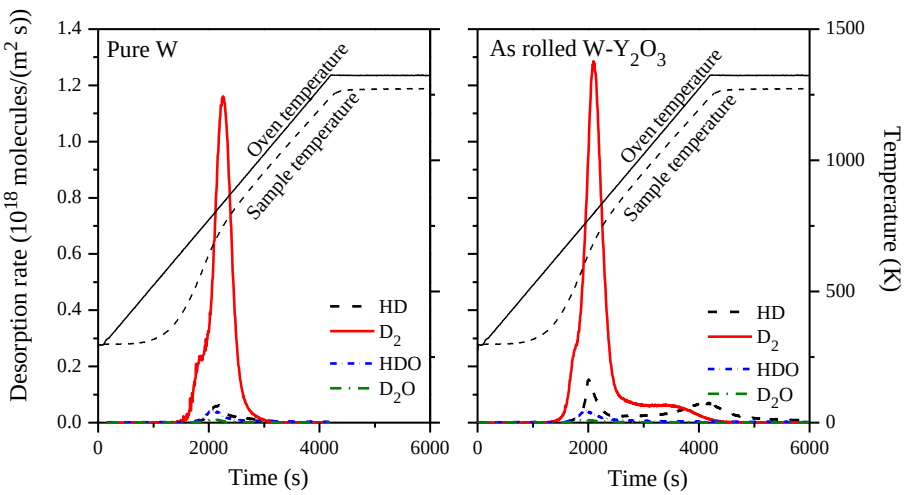


**Fig. 1:** Release rate of D-containing molecules as a function of time during TDS for pure W (left) and as-rolled W−$Y_2O_3$ (right) implanted at 38 eV/D incident energy with a fluence of $6\times10^{24}$ D/m$^2$ and a sample temperature of 450 K. The oven heating rate was 15 K/min, the oven and sample temperatures are shown on the right hand scale.

Representative TDS spectra—presented here are data for pure W and as-rolled W−$Y_2O_3$—attributed to D containing molecules (HD, $D_2$, HDO and $D_2O$) are shown in Fig. 1. The spectra shown in Fig. 1 as well as all other TDS spectra shown in this article are raw spectra, i.e. without background subtraction. The release rates of D-containing molecules are plotted as a function of elapsed time (left-hand scale). In addition, the oven and sample temperature ramps are also shown (right-hand scale). The contributions of heavy water (HDO and $D_2O$) and HD signals to the total D release are listed in Table 1. Deuterium released as $D_2$ plays a decisive role on the total D amounts for both pure W and W−$Y_2O_3$. On the contrary, HDO and $D_2O$ signals are very weak and nearly invisible. For pure W and as-rolled W−$Y_2O_3$ exposed at all investigated conditions, the absolute D amounts released in form of heavy water (HDO and $D_2O$) do not change significantly and range from $3.5\times10^{19}$ to $4.8\times10^{19}$ D/m$^2$. In general, they account for less than 10 % of the total D release. Here we should note again that the actual amount of D released as heavy water molecules could be higher due to the unknown loss of water to the chamber walls. For HD release spectra, as shown in Fig. 1, as-rolled W−$Y_2O_3$ shows not only a clear peak at about 640 K similar as pure W, but also a broad release peak in the high temperature region (higher than about 1000 K), yielding an about 3-times higher contribution to the total D release than for pure W. For as-rolled W−$Y_2O_3$ the HD release at high temperature (T > 1200 K) is accompanied by a release of $H_2$. The $H_2$ release rate is even higher than the HD release rate. A comparable $H_2$ release is not observed for pure W samples. Obviously, the initial sample preparation including baking at 1200 K for 2 hours (see Sect. 2.2) is not sufficient to remove all H trapped in W−$Y_2O_3$ during production. The deuterium released from pure W in form of HD contributes about 3−10 % to the total D amount. For as-rolled W−$Y_2O_3$, the contribution of HD signal to the total D release is about 12−15 % at low sample loading temperatures (370 and 450 K), and reaches surprisingly up to 31.3 % at high sample temperature (570 K). The appearance of the HD signal in the high temperature region for as-rolled W−$Y_2O_3$ is probably correlated with the presence of high energy trap sites, which is investigated in detail in sections 3.2.3 and 3.3.

## 3. Results and discussion

### 3.1. NRA depth profile

Fig. 2a shows the D depth profiles in the topmost 8 µm measured by NRA and evaluated using NRADC [20] (see section 2.3) for pure W and as-rolled W−$Y_2O_3$ implanted at 450 K with a low ($6\times10^{24}$ D/m$^2$) and high ($7.5\times10^{25}$ D/m$^2$) D fluence. Additionally shown are the accumulated D inventories as a function of depth in Fig. 2b. They were calculated from the D depth profiles by integration of the D amount from the surface to the given depth. The D depth profiles for the two investigated sample materials implanted at 370, 450 and 570 K with an incident fluence of $6\times10^{24}$ D/m$^2$ were previously published and shortly discussed in [10].

As shown in Fig. 2a, the shape of D depth profiles is very similar for both fluences. All D depth profiles – including those in Ref. [10] – exhibit a surface peak with a D concentration of the order of 1−4 %. For the two fluences investigated here, the surface D concentration is 1.5-2 % and quite comparable for W−$Y_2O_3$ and pure W. The surface peak is followed by a dip in the depth profile and by a local D concentration maximum in the depth range from 0.5 to 3.5 µm. After exposure with a fluence of $6\times10^{24}$ D/m$^2$, as reported in [10], both pure W and W−$Y_2O_3$ show a second D concentration maximum at about $2.7–2.9\times10^{-3}$ and then decrease to about $1\times10^{-3}$, reaching total D inventories of 9.5 and $9.4\times10^{20}$ D/m$^2$, respectively. In comparison, pure W and W−$Y_2O_3$ implanted with a fluence of $7.5\times10^{25}$ D/m$^2$, exhibit a

lower second D concentration maximum of around 2.0−2.2×$10^{-3}$ and maintain a lower D concentration at larger depth, resulting in lower total D inventories (pure W: 7.1×$10^{20}$ D/$m^2$, W−$Y_2O_3$: 6.6×$10^{20}$ D/$m^2$). A possible explanation for the lower local D concentration after the higher fluence (7.5×$10^{25}$ D/$m^2$) would be a possible bursting of blisters (see Sect. 3.2.2) or micro-cracking of the exposed surface, which would result in a stronger D loss due to "outgassing" [11,12].

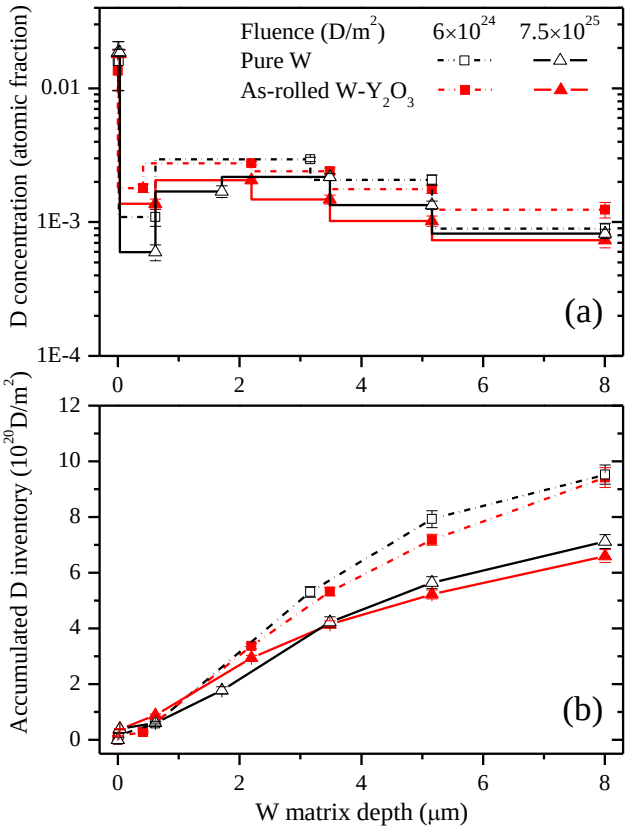


**Fig. 2:** D depth profiles (a) and the respective accumulated D inventories (b) versus depth for pure W and as-rolled W−$Y_2O_3$ after exposure at a low (6×$10^{24}$ D/$m^2$) and a high fluence (7.5×$10^{25}$ D/$m^2$) at 450 K. D depth profiles were determined by NRA. The accumulated D inventories were acquired by integrating the D amount from the surface to the respective depth. The shown error bars comprise only the statistical uncertainty from the raw data and the model evaluation from NRADC (see Sect.2.3).

## 3.2. TDS analysis

### 3.2.1. Deuterium retention

The total amount of deuterium measured by TDS ( $D_{TDS}$ ) was determined by integrating the signals of HD, $D_2$, HDO and $D_2O$ over time. To correct for the background contribution to the total D amount the integrated background contributions of the respective mass channels was subtracted from the integrated signal of the samples for the same period of time. For most samples this background subtraction corresponds to less than 2 % of the total released D amount. Only for the case with the lowest released D amount, the background subtraction corresponds to about 7 %. As discussed in section 2.4, the total uncertainty of $D_{TDS}$ is mainly due to the uncertainty in the evaluation of the HDO and $D_2O$ signals and a possible loss of deuterium during the additional storage time.

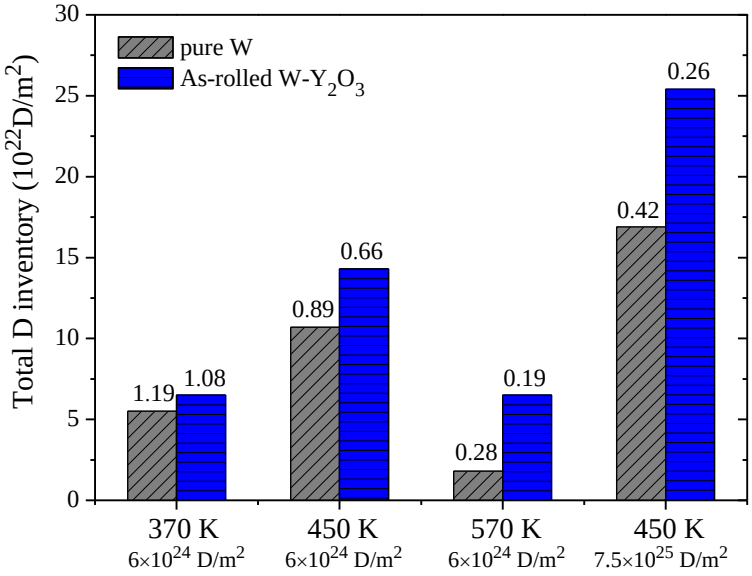


**Fig. 3:** Total amount of retained D determined by TDS in pure W and as-rolled W−$Y_2O_3$ after exposure to different fluences at different sample temperatures. The number above each column represents the fraction of the total D amount found within the NRA analysis depth of 8 µm. The precise data for total deuterium retention measured by NRA and TDS are listed in Table 1.

The total D amounts measured by NRA and TDS are summarized in Table 1 and presented in Fig. 3. Due to the limited information depth of NRA the D amount measured by NRA ($D_{NRA}$) is in general lower than the D amount measured by TDS [24]. To allow for a better comparison of the presented data the following two fractions are calculated and also listed in Table 1. $F_{NRA}$ is the fraction of the total retained D found within the NRA analysis depth ($F_{NRA} = D_{NRA}/D_{TDS}$). $F_Y$ is the ratio of the total D amount in as-rolled W−$Y_2O_3$ and in pure W ($F_Y = D_{W\text{-}Y2O3}/D_{pure\text{-}W}$) for the identical exposure condition. An $F_{NRA}$ value of 1 means that all D retained in the sample is found within the NRA analysis depth, while a value smaller than 1 indicates that a certain fraction is retained in a depth larger than the NRA analysis depth. $F_Y$ compares the D retention in pure W and as-rolled W−$Y_2O_3$.

For exposure at **370 K** $F_{NRA}$ is around 1. This indicates that for these exposure conditions almost all of the trapped deuterium is retained within the NRA information depth. The fact that the actual values are slightly higher than 1 is attributed to the uncertainty of the TDS analysis. Such a shallow penetration depth of deuterium in the samples exposed at this condition is further corroborated by the D depth profiles presented in [10] which show an exponential decrease of the local D concentration in the depth range between 2 and 8 µm. At 370 K, $D_{TDS}$ in as-rolled W−$Y_2O_3$ is $6.5\times10^{20}$ D/m$^2$, which is about 18 % higher than that of pure W ($5.5\times10^{20}$ D/m$^2$), i.e., $F_Y \approx 1.2$.

For exposure at **450 K**, $F_{NRA}$ is 0.89 and 0.66, respectively, which means a fraction of deuterium is retained in a depth larger than 8 µm. $D_{TDS}$ in pure W is 10.7 and in as-rolled W−$Y_2O_3$ $14.3\times10^{20}$ D/m$^2$. $F_Y$ is 1.3. After exposure at 450 K the retained D amounts are roughly a factor of 2 higher than those after exposure at 370 K. After the 12.5 times higher incident fluence of **$7.5\times10^{25}$ D/m$^2$**, $F_{NRA}$ decreases to 0.42 and 0.26, respectively, indicating that the dominant fraction of deuterium is in this case retained in a depth larger than 8 µm. Compared with the exposure to the lower fluence, as-rolled W−$Y_2O_3$ experienced a stronger increase in $D_{TDS}$ (by about +80 % to $25.4\times10^{20}$ D/m$^2$) than pure W (about +60 % to

$16.9\times10^{20}$ D/m$^2$). For these conditions the retention in as-rolled W−$Y_2O_3$ is about 50 % higher than in pure W (i.e., $F_Y$ = 1.5).

For exposure at **570 K**, $F_{NRA}$ is 0.28 and 0.20, respectively; suggesting that an even larger fraction of D is retained in a depth larger than 8 µm. $D_{TDS}$ in pure W is only one third of that at 370 K, while in as-rolled W−$Y_2O_3$ $D_{TDS}$ is surprisingly comparable with that at 370 K. For these conditions $F_Y$ = 3.6. Remarkable is the large relative contribution of heavy water to the total released D amount for this case (almost 20 %, see Table 1). In fact, the absolute contribution of heavy water is for all investigated cases comparable, but due to the much lower total released amount after exposure at 570 K, the relative contribution is very high. Similarly, the relative contribution of HD is high for this case. In general, the relative contribution of HD to the total released D amounts is significantly higher for W−$Y_2O_3$ than for pure W.

The dependence of D retention as a function of temperature is discussed to some more detail at the end of the following section 3.2.2. In addition, it is observed that at each investigated exposure condition pure W has an about 10−25 % higher $F_{NRA}$ value than as-rolled W−$Y_2O_3$. The local D concentrations of the two materials at the end of the NRA analysis range are comparable, but slightly lower for as-rolled W−$Y_2O_3$ (see [10] and Fig. 2a). This suggests a deeper penetration of deuterium in as-rolled W−$Y_2O_3$ than in pure W. But large cavities, such as the sub-micron pores in as-rolled W−$Y_2O_3$, should slow down the penetration of deuterium into tungsten samples [27]. In this regard we can speculate that $Y_2O_3$ particles might play a role in enhancing the penetration of deuterium. One possible explanation for this enhanced penetration could be that the $Y_2O_3$-W interfaces due to the presence of $Y_2O_3$ particles provide fast diffusion channels for implanted deuterium.

### 3.2.2. TDS spectra

The shape of the TDS spectra is influenced by the types (trap energies) and depth distributions of defects in the sample and additionally by the diffusion of D during heating. Much work has been performed in the past to relate trap energies to the observed desorption temperatures [28-32]. However, due to differences of the investigated samples and the used experimental set-ups published data show quite some scatter. Generally, deuterium released at lower temperature is attributed to deuterium trapped in low-energy trap sites (LET). The trap sites are either intrinsic defects or defects generated during deuterium loading. As discussed in section 2.4, the deuterium released as $D_2$ contributes in all investigated cases the largest fraction (between 60 and 95 %) to the total released D amount. In general, the shapes of the HD signals are very similar to the $D_2$ signals – they are just much lower. HDO and $D_2O$ signals are much weaker and on a linear scale nearly invisible compared with $D_2$ and HD signals. Therefore, in Fig. 4 we only present the $D_2$ release peaks as a function of the real sample temperature.

First we compare the spectra of the samples exposed to **the lower fluence of $6\times10^{24}$ D/m$^2$**, as shown in Fig. 4a. After exposure at 370 K pure W shows a main release peak at 720 K and a shoulder at about 500 K. As-rolled W−$Y_2O_3$ exhibits a slightly smaller main release peak at a lower temperature (635 K), a slightly bigger release shoulder at approximately the same temperature as pure W, and at temperatures above 760 K an additional long release tail. After exposure at 450 K, both materials show an almost identical release shoulder at about 500 K, but a 2 times bigger main release peak than after 370 K loading. In addition, the main release peaks of pure W and as-rolled W−$Y_2O_3$ are shifted to higher temperatures by 30 and 60 K, respectively. The intensity of the high temperature release tail of as-rolled W−$Y_2O_3$ increases proportionally to the main release peak. After exposure at 570 K, the shoulder at about 500 K

disappears for both tungsten materials the main release peak is strongly reduced and shifted to a higher temperature. On the contrary, the high temperature release tail of as-rolled W−$Y_2O_3$ is further strengthened and nearly 2 times as big as the main release peak.

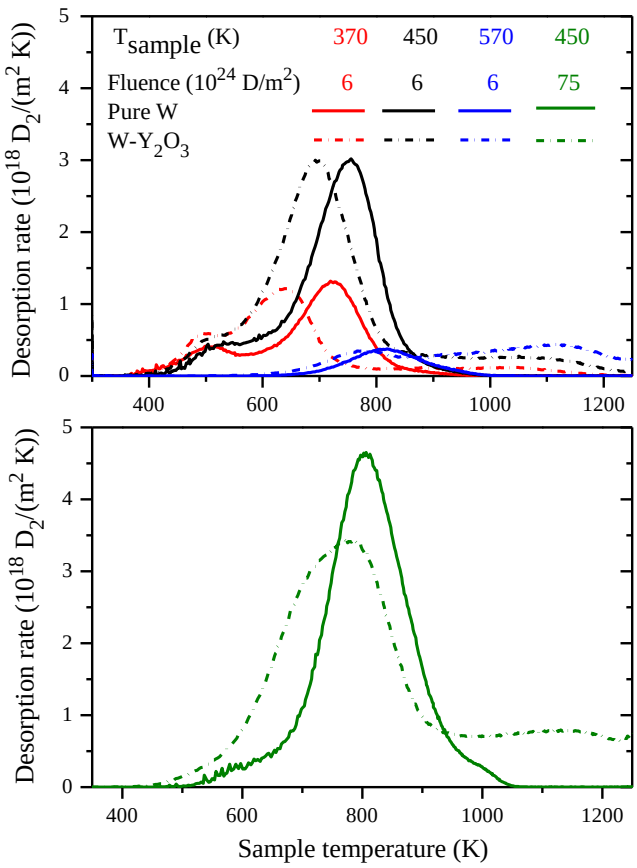


**Fig. 4:** $D_2$ release spectra of pure W and as-rolled W−$Y_2O_3$ exposed to a fluence of $6\times10^{24}$ and $7.5\times10^{25}$ D/m$^2$ at 370, 450 and 570 K, respectively. In all cases, the oven heating rate is 15 K/min.

An additional feature of the TDS spectra of pure W exposed at 370 and 450 K is the occurrence of sharp release peaks (spikes) in the low temperature region of the spectrum (between about 450 and 650 K). At first glance these features look as increased experimental noise, but they are not, as can be seen by comparison with the high temperature region of the spectra. It has been shown earlier that such spikes occurring in this temperature range are due to the bursts of gas-filled blisters [33]. In Ref. [33] the experimental parameters for the TDS measurements were optimized to make such blisters well visible. In the present measurements, the parameters are not optimal to make spikes clearly visible, but larger blisters still lead to the occurrence of visible spikes which cause the noisy appearance of the spectra for pure W. As reported in [10], as-rolled W−$Y_2O_3$ has much smaller blisters than pure W. The blisters in as-rolled W−$Y_2O_3$ are too small to cause visible spikes for the present experimental parameters.

The spectra of the samples exposed to **the higher fluence of $7.5\times10^{25}$ D/m$^{-2}$ at 450 K** are presented in Fig. 4b. For both materials the shoulder at low temperature has a slightly lower intensity, while the intensity of the main peak has increased. All peaks are shifted to higher temperatures. Particularly strong is the increase of the intensity of the high temperature release tail for as-rolled W−$Y_2O_3$. It should be noted that the release of D has not yet

terminated when the maximum temperature has been reached. It was already mentioned in Sect. 2.4 that the samples are held at $T_{max}$ for some additional time to allow for additional release of trapped D. This period is not shown in Fig. 4. During the holding at 1320 K – for 100 min in this case – the released D amount is about $3.3\times10^{20}$ D/m$^2$ for as-rolled W-$Y_2O_3$, corresponding to 13 % of the total D inventory. In comparison, $1.2\times10^{19}$ D/m$^2$ is released from pure W, accounting for only 0.7 % of the total D inventory. After the TDS measurements all samples were investigated by NRA once again. No D signals were detected, indicating complete removal of D from the bulk during TDS procedure.

The main differences for all $D_2$ release spectra between pure W and as-rolled W−$Y_2O_3$ are the positions of the main release peaks and the presence of an additional high temperature release in as-rolled W−$Y_2O_3$. The shoulder at lower temperatures and the main release peak in the range of 600 to 700 K are typical peaks reported for polycrystalline W [28,30,32,34,35]. For each investigated exposure condition as-rolled W−$Y_2O_3$ shows the main release peak at a lower temperature than pure W. Such a difference in peak position might be correlated to the $Y_2O_3$-W interface which might provide fast diffusion channels for deuterium release or it could be due to lower de-trapping energy in $Y_2O_3$-W. Unfortunately, we cannot prove any of these hypotheses at the moment. The appearance of the additional release tail in as-rolled W−$Y_2O_3$ suggests the presence of trap sites with high energies (HET), but their origin is still unclear. From the gradual increase of the $D_2$ amount released from HET's with the increase of D penetration depth due to higher $T_{sample}$ or due to higher incident fluence, we can conclude that these HET's are predominately intrinsic defects and are uniformly distributed in the bulk. Based on this conclusion, the high temperature $D_2$ release peak and the nature of the responsible HET's is further investigated in sections 3.2.3 and 3.3.

Considering the above discussion of the TDS analysis results presented in Figs. 3 and 4 and taking into account the D depth profiles measured by NRA after loading at different sample loading temperatures, $T_{sample}$, shown in Fig. 8 in Ref. [10] and in Fig. 2 in Sect. 3.1, the following conclusion can be drawn: At low sample loading temperatures ($T_{sample}$ = 370 and 450 K), deuterium release is dominated by release in the low-temperature region. This includes the low-temperature shoulder (around 500 K) and the main peak (630 to 750 K). These D release peaks contribute between 60 and 95 % to the total D inventory. At 370 K, D has penetrated up to the end of the NRA analysis range of about 8 µm. This results in a $F_{NRA}$ value of around 1 (see Tab. 1). After loading at 450 K, D has penetrated deeper resulting in a $F_{NRA}$ value of below 1 (see Tab. 1). TDS results (Fig. 4) indicate a comparable contribution of LET's to total retention and NRA depth profiles (see Fig. 2 above and Fig. 8 in Ref. [10]) show a comparable local D concentration. The increase of the total D amount at 450 K is, therefore, explained by a deeper penetration of D due to higher diffusivity at higher temperature. Assuming that the local D concentration at the end of the NRA measuring range extents further into depth we can estimate the 'D-filled range' from a comparison of NRA and TDS data. The D concentrations for pure W and W-Y2O3 exposed at 450 K to the higher fluence of $7.5\times10^{25}$ D/m$^{-2}$ are $8.2\times10^{-4}$ and $7.3\times10^{-4}$, respectively (see Fig. 2a). The corresponding differences between NRA and TDS amounts are 9.8 and $18.8\times10^{20}$ m$^{-2}$, respectively (see Tab. 1). This estimate results in D penetration ranges of about 30 and 50 µm (including the top 8 µm analysed by NRA). Of course, penetration ranges will be larger if we assume a decrease of the local concentration with increasing depth.

At high $T_{sample}$ (570 K), D release from the high-temperature region is dominant (60−70 %). In other words, most deuterium is trapped by LET at low $T_{sample}$ and by HET at high $T_{sample}$. The lower total D retention at 570 K (see Fig. 3) is due to the thermal detrapping of D from LET's during plasma loading, which leads to a lower local D concentration as shown by the NRA depth profiles. At the same time, the local D concentration for as-rolled W−$Y_2O_3$ shown

by the D depth profiles is at low temperature comparable with that for pure W while at high $T_{sample}$ it is 2−3 times higher. This higher local concentration can be clearly attributed to the presence of HET's. For conditions where the total retention is increased due to deep diffusion into the bulk (i.e., at higher temperature and at higher impinging D fluences), these HET's lead to a significantly higher retention for as-rolled W−$Y_2O_3$ than for pure W.

### 3.2.3. High temperature release peak

As shown in section 3.2.2, one of the main differences between pure W and as-rolled W−$Y_2O_3$ is the additional high temperature release for the latter which was attributed to the presence of HET's in as-rolled W−$Y_2O_3$. The objective of this section is to determine the total D amount trapped by these HET's by ramp-and-hold experiments in TESS (see Fig. 5) and measure the local concentration of D trapped by HET within the NRA information depth (see Fig. 6) after a ramp-and-hold experiment at 840 K. Ramp-and-hold experiments means that a sample is ramped with a given heating ramp to a certain temperature, held there for a certain time and then cooled down again.

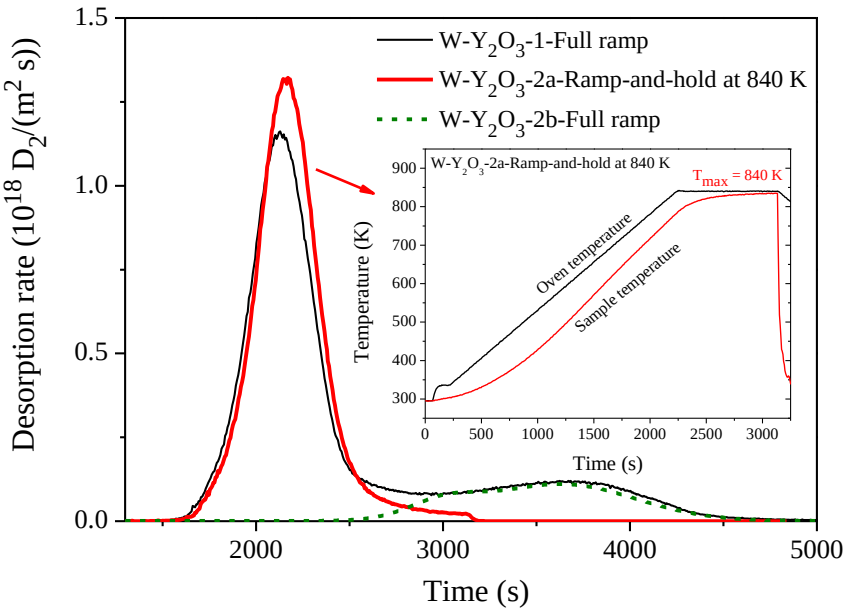


**Fig. 5:** $D_2$ release spectra of two identical as-rolled W−$Y_2O_3$ specimens (W−$Y_2O_3$-1 and W−$Y_2O_3$-2). The $D_2$ release spectrum of W−$Y_2O_3$-1 (black solid line) was obtained by a full ramp up to 1320 K. W−$Y_2O_3$-2 was subjected to two TDS experiments. The corresponding spectra are denoted as W−$Y_2O_3$-2a and W−$Y_2O_3$-2b, respectively. The $D_2$ release spectrum of W−$Y_2O_3$-2a (red solid line) was obtained by a ramp-and-hold experiment at 840 K (for details see text). The temperature program for this experiment is shown in the inset. The $D_2$ release spectrum of W−$Y_2O_3$-2b (green dashed line) was obtained by a full ramp up to 1320 K.

Two as-rolled W−$Y_2O_3$ samples (denoted as W−$Y_2O_3$-1 and W−$Y_2O_3$-2) randomly cut from the same rolling plate as the samples used for the experiments discussed so far were exposed simultaneously at 450 K with an incident fluence of $6\times10^{24}$ D/m$^2$ and ion energy of 38 eV/D. The D depth profiles of these two samples were determined by NRA. The two identical W−$Y_2O_3$ samples show a comparable D depth profile. Fig. 6 displays the D depth profile of W−$Y_2O_3$-2 as a representative. It is worth mentioning that the D depth profiles and total D inventories of these two samples are within experimental uncertainty in excellent agreement with the data used in Table 1 and the depth profile shown in Fig. 2. After D

loading, W−$Y_2O_3$-1 was subjected to a full ramp experiment up to $T_{max}$ (1320 K, see Section 2.4) for obtaining the total D inventory, W−$Y_2O_3$-2 was subjected to a ramp-and-hold experiment at 840 K, which is shown as an inset in Fig. 5. Herein, the W−$Y_2O_3$-2 sample after the deuterium implantation is named W−$Y_2O_3$-2a and the same sample after performing the ramp-and-hold experiment at 840 K is named W−$Y_2O_3$-2b. The $D_2$ release spectra of W−$Y_2O_3$-1 and W−$Y_2O_3$-2a are plotted as black and red solid lines in Fig. 5, respectively. The deuterium retention in W−$Y_2O_3$-1 and W−$Y_2O_3$-2a was measured once again by NRA and TDS. No D signal was detected on W−$Y_2O_3$-1 after the full ramp experiment both by NRA and TDS. For W−$Y_2O_3$-2b, the D depth profile and $D_2$ release spectrum are shown as red solid line in Fig. 6 and as green dashed line in Fig. 5, respectively. The sum of the $D_2$ release spectra of W−$Y_2O_3$-2a and W−$Y_2O_3$-2b is almost identical to the spectrum of W−$Y_2O_3$-1. The remaining difference is attributed to the general experimental uncertainty. This research result, on the one hand, proves the uniformity of microstructure of the investigated W−$Y_2O_3$ rolling plate, and, on the other hand, it reveals that the used ramp-and-hold experiment at 840 K released almost all of the D trapped by LET's.

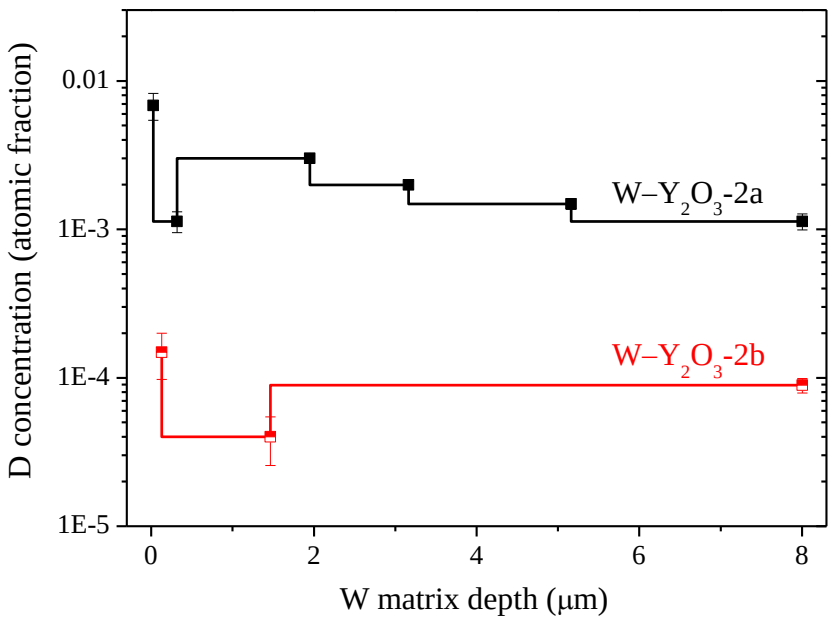


**Fig. 6:** D depth profiles (topmost 8 μm) for W−$Y_2O_3$-2 specimen. The black line shows the local D concentration after exposure to D plasma with a fluence of $6\times10^{24}$ D/m$^2$ at 450 K(sample W−$Y_2O_3$-2a in Fig. 5). The red line shows the local D concentration after the first ramp up to 840 K (sample W−$Y_2O_3$-2b in Fig. 5). The shown error bars comprise only the statistical uncertainty from the raw data and the model evaluation from NRADC (see Sect.2.3).

We should further note that this experiment shows that the TDS spectra represent a distribution of binding energies, because there is no redistribution of D in the sample during the ramp to 840 K. In other words: LET's which become depopulated in the first ramp up to 840 K do not become repopulated during cooling or the following heating phase. During the second full ramp up to 1320 K, D from the high energy traps is released and this release is not influenced by the prior annealing to 840 K. The TDS experiment on W−$Y_2O_3$-2b shows that the total amount of D from HET's is about $4.2\times10^{20}$ D/m$^2$, contributing around 30 % of the total D inventory in as-rolled W−$Y_2O_3$. Fig. 6 clearly shows that D trapped by HET's is uniformly distributed in the depth ranging from 1.5 to 8 μm with a concentration of $8.9\times10^{-5}$.

This concentration could be considered as the "equilibrium concentration" of D in HET's for exposure at 450 K. Assuming that the local D concentration trapped by HET's at larger depth of as-rolled W−$Y_2O_3$ specimen is constant and equal to this concentration, we can estimate the penetration depth of D from the retained total amount. Under the given plasma exposure and temperature conditions the D penetration depth into the as-rolled (W−$Y_2O_3$) specimen is estimated to be of the order of 100 µm. However, it cannot be excluded, that to some extent this deep penetration occurred during the ramp-and-hold experiment.

### 3.3. Nature of high energy trap sites

The investigation in this section aims at the understanding of the nature of HET sites in as-rolled W−$Y_2O_3$. The intrinsic defects with high trapping energies in as-rolled W−$Y_2O_3$ could be $Y_2O_3$ itself or/and the $Y_2O_3$-W interface or/and residual pores as discussed in [10]. Fig. 7 shows the $D_2$ release spectra of the three different used W−$Y_2O_3$ materials after simultaneous exposure at 570 K with an incident fluence of $6\times10^{24}$ D/m$^2$. As the total release of D is dominated by $D_2$ (the fraction varies between 63 and 84 %) only the mass 4 spectra are shown in Fig. 7. Similar as in Fig. 4 the release of D has not yet terminated for some samples when the maximum temperature has been reached and as mentioned in Sect. 2.4 and shown in Fig. 1 the samples were held at $T_{max}$ for some additional time. These data are not included in Fig. 7. During the holding at 1320 K for more than one hour, the released D amounts from as-sintered, as-rolled and SPS-ed W−$Y_2O_3$ is 2.44, 1.45 and $0.14\times10^{20}$ D/m$^2$, respectively. These values account for 29, 22 and 4.6 % of the corresponding total D inventories, respectively. As shown in Fig. 1, the $D_2$ and HD release signals did not really reach zero for as-sintered and as-rolled W−$Y_2O_3$ samples even after holding at 1320 K for 120 min. Therefore, after the full-ramp TDS experiments (including the extended holding at $T_{max}$), we conducted a second round of NRA and TDS measurements on these samples. However, most probably because the remaining D amounts lay below the detection limits of the two measuring techniques, no D signals were detected. This means that the D amounts remaining in as-sintered and as-rolled W−$Y_2O_3$ samples after TDS analysis are negligible.

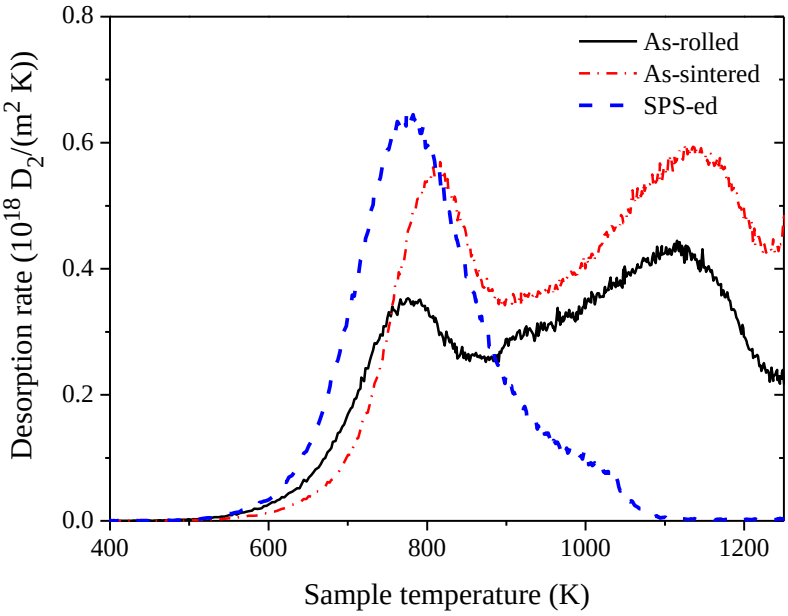


**Fig. 7:** $D_2$ release spectra of as-rolled, as-sintered and SPS-ed W−$Y_2O_3$ samples exposed to a fluence of $6\times10^{24}$ D/m$^2$ at 570 K. In all cases, the oven heating rate is 15 K/min.

The three different W−$Y_2O_3$ materials shown in Fig. 7 are as-sintered one, as-rolled one and SPS-ed one, respectively. Detailed production routes and microstructural characteristics were summarized in section 2.1. All of these W−$Y_2O_3$ materials have the same amount of $Y_2O_3$. In terms of W grain boundaries and $Y_2O_3$-W interfaces, SPS-ed W−$Y_2O_3$ has more than as-sintered and as-rolled W−$Y_2O_3$, which have approximately the same. As to porosity, SPS-ed W−$Y_2O_3$ is identical to as-rolled W−$Y_2O_3$ (0.7 %), but slightly lower than as-sintered W−$Y_2O_3$ (1.1 %). Furthermore, the SPS-ed W−$Y_2O_3$ has nano cavities (Fig. 8c) while both as-sintered and as-rolled W−$Y_2O_3$ have sub-micron pores (see [8,10]). From Fig. 7 SPS-ed W−$Y_2O_3$ is observed to show no obvious high temperature $D_2$ release peak. As-sintered W−$Y_2O_3$ shows a similar shape of $D_2$ release spectrum as as-rolled W−$Y_2O_3$, but its spectrum intensity is stronger than the latter. From this we conclude that the appearance of the high temperature release peak in as-rolled W−$Y_2O_3$ is neither directly correlated with the amount of $Y_2O_3$ (all specimen have the identical amount) nor with the extent of the $Y_2O_3$-W interface (which is largest for SPS-ed W−$Y_2O_3$), but is probably related to the presence of visible, sub-micron pores. We further conclude that the size and volume percentage of pores are key factors for the retention capability.

Hydrogen isotopes retention in W materials depends on the microstructure which is largely determined by the production history [13,14]. A. Manhard et al. have shown that a modification of the initial microstructure of the investigated tungsten grade has a big influence on the measured D retention [35]. The observed difference in the $D_2$ release peaks between SPS-ed and as-sintered W−$Y_2O_3$ could be induced by some unnoticed difference in microstructure due to the used different sintering techniques. In the following experiment we, therefore, studied the deuterium retention behavior of two SPS-ed W−$Y_2O_3$ samples after simultaneous exposure at 450 K with an incident fluence of $6\times10^{24}$ D/m$^2$ by NRA and TDS. The two used SPS-ed W−$Y_2O_3$ samples were from the same production batch, as the one used above (see Fig. 7). Prior to deuterium implantation, one of the samples was annealed at 2170 K for 3 h in a vacuum oven with a base pressure of about $2\times10^{-6}$ Pa. Fig. 8 shows the microstructure of SPS-ed W−$Y_2O_3$ with and without annealing. For each sample, two images are presented. Scanning electron microscopy (SEM, HELIOS NanoLab 600) and transmission electron microscopy (TEM, JEOL JEM-2010) were used to characterize the microstructure of the two different SPS-ed W−$Y_2O_3$. Due to annealing, the average grain size increases and the density of tungsten−$Y_2O_3$ grain boundaries decreases (Figs. 8a and 8b), new pore structures with diameters of several hundred nm appear and accumulate at $Y_2O_3$-W interfaces (Fig. 8d). These new submicron pores could be formed either by the accumulation of nano cavities located at tungsten grain boundaries (Fig. 8c) or by the movement and clustering of volume defects such as vacancies, voids and dislocations. On the one hand, it was reported that the reduction in the density of grain boundaries will cause the decrease of local D concentration and the total D inventory [35] and, on the other hand, it was shown that pore structures provide new trapping sites which obviously increase the retained D amount [27]. Fig. 9 shows the D depth profiles of the respective accumulated D inventories for SPS-ed W−$Y_2O_3$ with and without annealing. Unexpectedly the sample after annealing exhibits a higher local D concentration within the NRA information depth than the sample without annealing ($20.6\times10^{20}$ D/m$^2$ vs. $13.6\times10^{20}$ D/m$^2$, see also Tab. 1). Furthermore, the local D concentration in the topmost 3 µm is substantially higher than the concentration in as-rolled W−$Y_2O_3$ (see Figs. 2 and 6) and the decrease of the depth profile with larger depth is much steeper than for the other shown cases. This means that for the given loading conditions for the data shown in Fig. 9 most of the retained D is found within the topmost 5 µm, i.e., well within the NRA analysis depth.

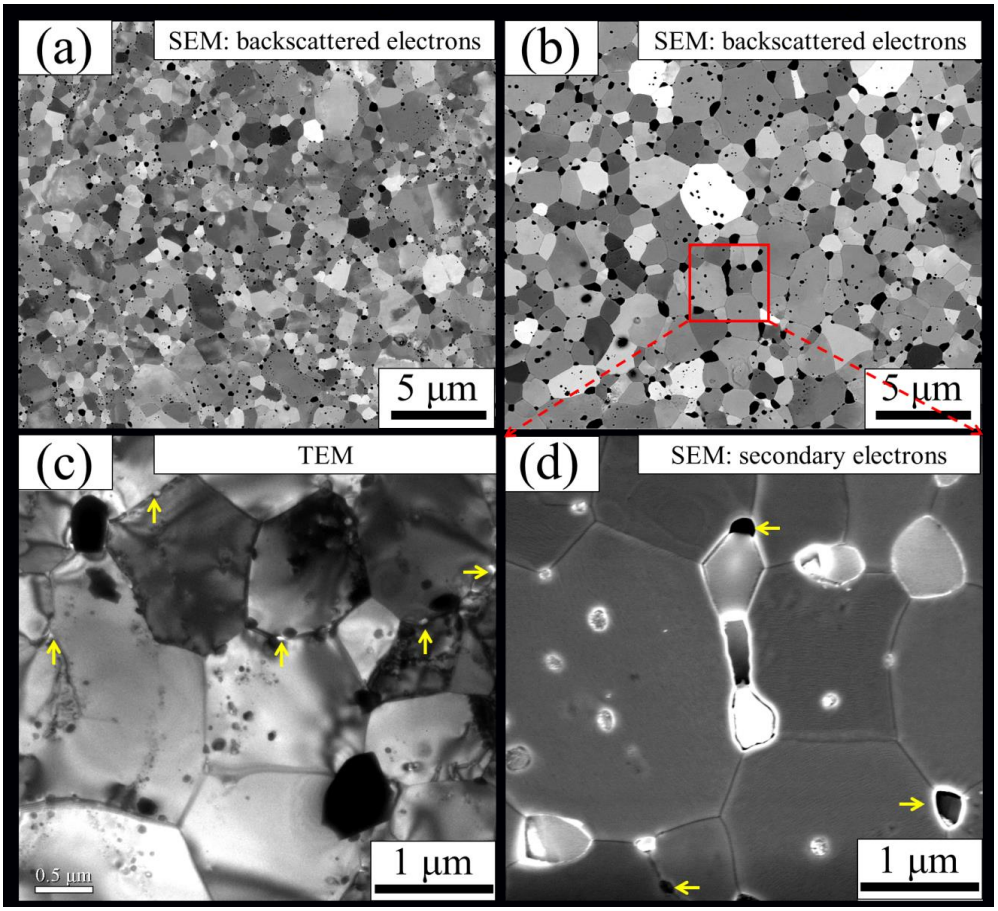


**Fig. 8:** (a) and (c) SPS-ed W−$Y_2O_3$ without annealing, (b) and (d) SPS-ed W−$Y_2O_3$ with annealing. (a), (b), and (d) are SEM images; (c) is a TEM image. Annealing was conducted at 2170 K for 3 h in a high vacuum oven. Residual pores in the samples are marked by yellow arrows. The black areas in (a)-(c) and white areas in (d) are $Y_2O_3$ particles.

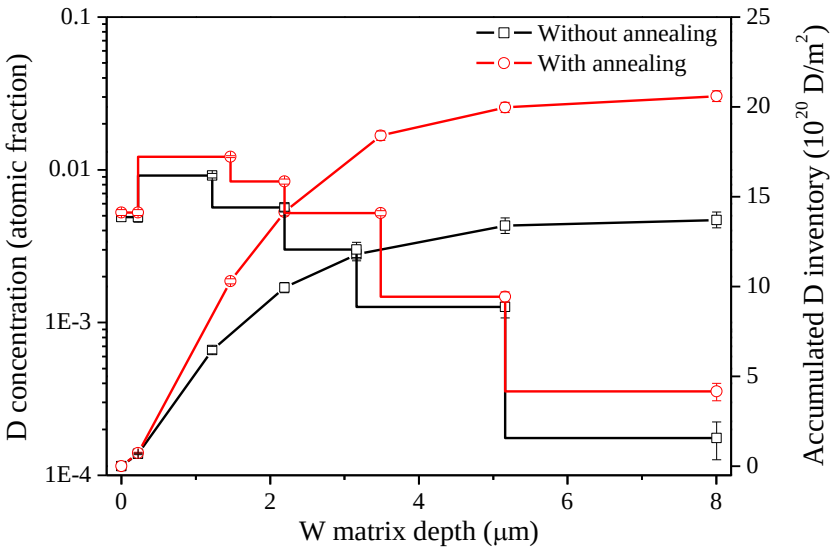


**Fig. 9:** D depth profiles (topmost 8 µm) and the respective accumulated D inventories versus depth for SPS-ed W−$Y_2O_3$ with and without annealing after exposure to a low fluence of $6\times10^{24}$ D/m$^2$ at 450 K. The shown error bars comprise only the statistical uncertainty from the raw data and the model evaluation from NRADC (see Sect.2.3).

The $D_2$ release spectra as a function of sample temperature for these two samples are displayed in Fig. 10. In comparison to the not annealed sample, the $D_2$ release spectrum for the annealed sample is characterized by an additional broad $D_2$ release peak centered at about 1100 K. Similar to Fig. 1, an additional HD release spectrum at high temperatures is also found for the annealed sample (not shown). The total D inventories determined from the TDS spectra are $14.4\times10^{20}$ D/m$^2$ for the not annealed sample and $20.4\times10^{20}$ D/m$^2$ for the annealed sample. They are in good agreement with the D inventories determined by NRA (see Fig. 9 and Tab. 1). This observation is consistent with the D depth profiles shown in Fig. 9 which have shown that most D is retained within the topmost 5 µm. The higher D retention for the annealed sample corresponds to an increase by about 50 %. The D amounts released as $D_2$ contribute about 94 and 96 % of the total D inventories for the not annealed sample and annealed samples, respectively.

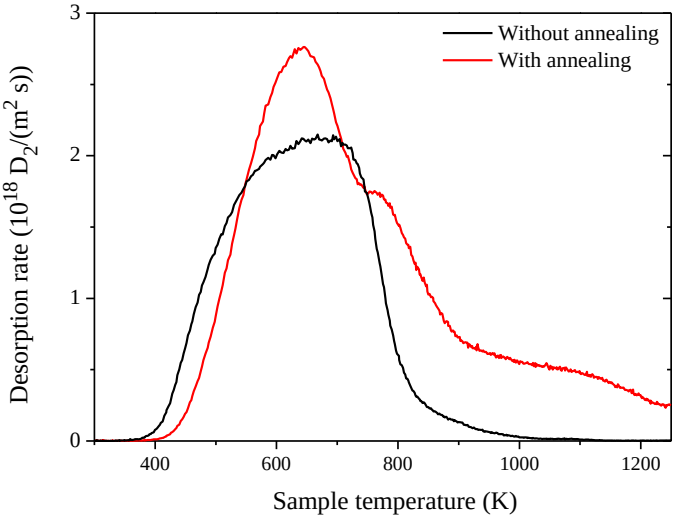


**Fig. 10:** $D_2$ release spectra of SPS-ed W−$Y_2O_3$ with and without annealing after exposure at 450 K with an incident fluence of $6\times10^{24}$ D/m$^2$.

To quantify the amount of D trapped in the additional high temperature release peak the $D_2$ release spectra measured as a function of time were fitted by a multi-peak Gaussian fit (not shown). The Gaussian-fitted spectra fit the experimental $D_2$ release rates very well and allow a good quantification of the contribution of the individual peaks. The contribution of the additional high temperature $D_2$ and HD peaks for the annealed sample is $5.4\times10^{20}$ D/m$^2$. This contributes about 28 % to its total D inventory. This means that the higher retention in the sample after annealing is more or less completely due to the additional release peak. From the quantitative analysis above, we conclude that the higher local D concentration for SPS-ed W−$Y_2O_3$ with annealing (Fig. 9) is correlated with the appearance of the high temperature $D_2$ and HD release peaks. In combination with the microstructural observation (Fig. 8), we, therefore, attribute the appearance of the high temperature $D_2$ and HD release peaks after annealing to the formation of submicron pores and conclude that sub-micron pores are intrinsic defects with high trapping energy.

## 4. Summary

Deuterium was implanted into pure W and as-rolled W−$Y_2O_3$ samples using the laboratory plasma experiment PlaQ. The implantation parameters were: ion energy 38 eV/D, sample temperature ($T_{sample}$) 370, 450 and 570 K, and applied fluence $6\times10^{24}$ and $7.5\times10^{25}$ D/m$^2$. The deuterium retention behavior of exposed pure W and as-rolled W−$Y_2O_3$, which have a similar

production process and thus similar tungsten grain morphology, was investigated and compared by nuclear reaction analysis and thermal desorption spectroscopy. D depth profiles determined by nuclear reaction analysis are comparable for pure W and as-rolled $W-Y_2O_3$ after exposure at 450 K with high fluence. At each investigated exposure condition, the fraction of D amount measured by nuclear reaction analysis relative to the total D amount measured by thermal desorption spectroscopy is lower for as-rolled $W-Y_2O_3$ than for pure W, indicating a larger diffusion depth of implanted D into $W-Y_2O_3$ than into pure W. One of the main differences in deuterium release spectra between pure W and as-rolled $W-Y_2O_3$ is an additional high-temperature release of HD and $D_2$ for as-rolled $W-Y_2O_3$. For exposure at low $T_{sample}$ (370 and 450 K), about 60−95 % deuterium are from low temperature release, i.e, low energy trap sites. While for exposure at high $T_{sample}$ (570 K), deuterium released from high energy trap sites in as-rolled $W-Y_2O_3$ contributes 60~70 % to the total D inventory. As a consequence, as-rolled $W-Y_2O_3$ shows after exposure at 370 and 450 K a comparable local D concentration, having only 20−50 % difference in total D inventory with pure W. While after exposure at 570 K, as-rolled $W-Y_2O_3$ shows 2−3 times higher local D concentration, causing about 3.6 times larger total D inventory than pure W.

In the late 90's, there were some studies of D retention in $La_2O_3$-doped tungsten [36,37]. A detailed comparison with the here presented results is difficult due to the very different exposure conditions. Nevertheless, a few general trends can be compared: Both studies show no dramatic increase of H isotope retention in the oxide particle doped W material compared with pure W. The retained amounts are slightly higher for the doped W and retention increased with increasing temperature, show a maximum at about 500 K [36] or 700 K [37] and steeply decrease for higher loading temperatures. The general trends as well as the reported absolute retained amounts are in reasonable agreement with the results presented in this work. The TDS release peaks for the $La_2O_3$-doped tungsten are reported to be in the range 500 to 1400 K [37] depending on loading conditions and the TDS spectra show a clear indication of a high temperature release peak which becomes stronger populated at higher loading temperatures. This is similar to the observations in this work which show a high temperature release peak up to temperatures of 1200 K.

The local concentration and total amount of D retained in high energy trap sites of as-rolled $W-Y_2O_3$ exposed at 450 K with an incident fluence of $6\times10^{24}$ D/m$^2$ was roughly determined by proper ramp-and-hold experiments in the TESS set-up. The results show that the D released from the high energy trap sites contributes around 30 % to the total D inventory in the bulk and that the concentration of D retained in high energy trap sites is constant at $8.9\times10^{-5}$ in the depth range between 1.5 and 8 μm. The later value is considered as "equilibrium concentration" of D in the high energy traps for loading at 450 K.

For understanding the nature of high energy trap sites in as-rolled $W-Y_2O_3$, we investigated and compared the deuterium retention behavior of four different $W-Y_2O_3$ samples, which have the same amount of $Y_2O_3$ particles but different microstructures. The results show that sub-micron pore structures are the underlying intrinsic defects which lead to the high-temperature D release in as-rolled $W-Y_2O_3$.

**Acknowledgments**

The stay of M. Zhao at Max Planck Institute for Plasma Physics in Garching was made possible through the financial support of the Chinese Scholarship Council which is gratefully acknowledged. We would further like to thank Rupert Brüderl for the help with sample preparation, Gabriele Matern for the help with the SEM investigations, Klaus Schmid for the help with evaluation of the ion beam measurements, and Thomas Schwarz-Selinger for the help with arrangement of the TDS.

## References


[1] R. Aymar, ITER status, design and material objectives, J. Nucl. Mater. **307–311** (2002) 1–9.

[2] R. Neu, V. Bobkov, R. Dux, A. Kallenbach, Th. Pütterich, H. Greuner, O. Gruber, A. Herrmann, Ch. Hopf, K. Krieger, C.F. Maggi, H. Maier, M. Mayer, V. Rohde, K. Schmid, W. Suttrop, Final steps to an all tungsten divertor tokamak, J. Nucl. Mater. **363–365** (2007) 52–59.

[3] V. Barabash, A. Peacock, S. Fabritsiev, G. Kalinin, S. Zinkle, A. Rowcliffe, J.-W. Rensman, A.A. Tavassoli, P. Marmy, P.J. Karditsas, F. Gillemot, M. Akiba, Materials challenges for ITER–Current status and future activities, J. Nucl. Mater. **367–370** (2007) 21–32.

[4] M.R. Gilbert, J.–Ch. Sublet, Neutron–induced transmutation effects in W and W-alloys in a fusion environment, Nucl. Fusion **51** (2011) 043005.

[5] X. Liu, J.M. Chen, Y.Y. Lian, J.H. Wu, Z.Y. Xu, N.M. Zhang, Q.M. Wang, X.R. Duan, Z.H. Wang, J.M. Zhong, Vaccum hot-pressed beryllium and TiC dispersion strengthened tungsten alloy developments for ITER and future fusion reactors, J. Nucl. Mater. **442** (2013) S309–S312.

[6] L.M. Luo, X.Y. Tan, H.Y. Chen, G.–N. Luo, X.Y. Zhu, J.G. Cheng, Y.C. Wu, Preparation and characteristics of W–1 wt.% TiC alloy via a novel chemical method and spark plasma sintering, Powder Technol. **273** (2015) 8–12.

[7] J. Riesch, J.–Y. Buffiere, T. Höschen, M. Di Michiel, Ch. Linsmeier, J.–H. You, In situ synchrotron tomography estimation of toughening effect by semi-ductile fibre reinforcement in a tungsten-fibre-reinforced tungsten composite system, Acta Mater. **61** (2013) 7060–7071.

[8] M. Zhao, Z. Zhou, M. Zhong, J. Tan, Effect of hot rolling on the microstructure and fracture behavior of a bulk fine-grained W–$Y_2O_3$ alloy, Mater. Sci. Eng. A **646** (2015) 19–24.

[9] M. Zhao, Z. Zhou, M. Zhong, J. Tan, Y. Lian, X. Liu, Thermal shock behavior of fine grained W–$Y_2O_3$ materials fabricated via two different manufacturing technologies, J. Nucl. Mater. **470** (2016) 236–243.

[10] M. Zhao, W. Jacob, A. Manhard, L. Gao, M. Balden, U. von Toussaint, Z. Zhou, Deuterium implantation into $Y_2O_3$-doped and pure tungsten: deuterium retention and blistering, J. Nucl. Mater. **487** (2017) 75-83.

[11] L. Gao, U. von Toussaint, W. Jacob, M. Balden, A. Manhard, Suppression of hydrogen-induced blistering of tungsten by pre-irradiation at low temperature, Nucl. Fusion **54** (2014) 122003.

[12] J. Bauer, T. Schwarz-Selinger, K. Schmid, M. Balden, A. Manhard, U. von Toussaint, Influence of near-surface blisters on deuterium transport in tungsten, Nucl. Fusion **57** (2017) 086015.

[13] M. Balden, A. Manhard, S. Elgeti. Deuterium retention and morphological modifications of the surface in five grades of tungsten after deuterium plasma exposure, J. Nucl. Mater. **452** (2014) 248–256.

[14] A. Manhard, Deuterium Inventory in Tungsten after Plasma Exposure: A. Microstructural Survey (Ph.D. Thesis, University Augsburg), Technical Report IPP 17/34, Garching 2012, Web link: http://hdl.handle.net/11858/00-001M-0000-0026-E65B-C

[15] M. Zhao, Z. Zhou, Q. Ding, M. Zhong, K. Arshad, Effect of rare earth elements on the consolidation behavior and microstructure of tungsten alloys, Int. J. Refract. Met. Hard Mater. **48**(2015) 19-23.

[16] M. Zhao, Z. Zhou, Q. Ding, M. Zhong, J. Tan, The investigation of Y doping content effect on the microstructure and microhardness of tungsten materials, Mat. Sci. Eng. A **618** (2014) 572-577.

[17] A. Manhard, G. Matern, M. Balden, A step-by-step analysis of the polishing process for tungsten specimens, Practical Metallogr. **50** (2013) 5–16.

[18] A. Manhard, T. Schwarz–Selinger, W. Jacob, Quantification of the deuterium ion fluxes from a plasma source, Plasma Sources Sci. Technol. **20** (2011) 015010.

[19] V.Kh. Alimov, M. Mayer, J. Roth, Differential cross section of the D($^3$He,p)$^4$He nuclear reaction and depth profiling of deuterium up to large depths, Nucl. Instrum. Meth. B **234** (2005) 169–175.

[20] K. Schmid, U. von Toussaint, Statistically sound evaluation of trace element depth profiles by ion

beam analysis, Nucl. Instrum. Meth. B **281** (2012) 64–71.

[21] S. Bielesch, M. Oberkofler, H.–W. Becker, H. Maier, D. Rogalla, T. Schwarz Selinger, C. Linsmeier, Experimental resolution of deuterium and hydrogen depth profiling with the nuclear reactions D($^{3}$He, p)α and p($^{15}$N, α, γ)$^{12}$C, Nucl. Instrum. Meth. B **317** (2013) 121–125.

[22] E. Salançon, T. Dürbeck, T. Schwarz-Selinger, F. Genoese, W. Jacob, Redeposition of amorphous hydrogenated carbon films during thermal decomposition, J. Nucl. Mater. **376** (2008) 160-168.

[23] K.A. Moshkunov, K. Schmid, M. Mayer, V.A. Kurnaev, Yu.M. Gasparyan, Air Exposure and Sample Storage Time Influence on Hydrogen Release from Tungsten, J. Nucl.Mater. **404** (2010) 174-177.

[24] P. Wang, W. Jacob, L. Gao. T. Dürbeck, T. Schwarz-Selinger, Comparing deuterium retention in tungsten films measured by temperature programmed desorption and nuclear reaction analysis, Nucl. Instrum. Meth. B **300** (2013) 54-61.

[25] A. Cornu, R. Massot, Compilation of Mass Spectral Data, second ed., Heyden & Son, vol. 1, Part A, 1979.

[26] <http://www.hidenanalytical.com/index.php/en/cracking-patterns>

[27] P. Wang, W. Jacob, S. Elgeti, Deuterium retention in tungsten films after different heat treatments, J. Nucl. Mater. **456** (2015) 192-199.

[28] K. Schmid, V. Rieger, A. Manhard, Comparison of Hydrogen Retention in W and W/Ta Alloys, J. Nucl. Mater. **426** (2012) 247-253.

[29] M. Poon, A.A. Haasz, J.W. Davis, Modelling deuterium release during thermal desorption of $D^{+}$-irradiated tungsten, J. Nucl. Mater. **374** (2008) 390-402.

[30] O.V. Ogorodnikova, J. Roth, M. Mayer, Ion-driven deuterium retention in tungsten, J. Appl. Phys. **103** (2008) 034902.

[31] W.R. Wampler, R.P. Doerner, The influence of displacement damage on deuterium retention in tungsten exposed to plasma, Nucl. Fusion **49** (2009) 115023.

[32] M.H.J. ‘t Hoen, B. Tyburska-Püschel, K. Ertl, M. Mayer, J. Rapp, A.W. Kleyn, P.A. Zeijlmans van Emmichoven, Saturation of deuterium retention in self-damaged tungsten exposed to high-flux plasmas, Nucl. Fusion **52** (2012) 023008.

[33] A. Manhard, U. von Toussaint, T. Dürbeck, K. Schmid, W. Jacob, Statistical Analysis of Blister Bursts during Temperature Programmed Desorption of Deuterium-implanted Polycrystalline Tungsten, Phys. Scr. **T145** (2011) 014038.

[34] W.M. Shu, E. Wakai, T. Yamanishi, Blister bursting and deuterium bursting release from tungsten exposed to high fluences of high flux and low energy deuterium plasma, Nucl. Fusion **47** (2007) 201-209.

[35] A. Manhard, K. Schmid, M. Balden, W. Jacob, Influence of the Microstructure on the Deuterium Retention in Tungsten, J. Nucl. Mater. **415** (2011) S632-S635.

[36] A.A. Haasz, J.W. Davis, M. Poon, R.G. Macaulay-Newcombe, Deuterium retention in tungsten for fusion use, J. Nucl. Mater. **258-263** (1998) 889-895.

[37] R. Causey, K. Wilson, T. Venhaus, W. R. Wampler, Tritium retention in tungsten exposed to intense fluxes of 100 eV tritons, J. Nucl. Mater. **266-269** (1999) 467-471.